The Swelling Behaviour of Thermoresponsive Hydrogel-Silica Nanoparticle Composites

Coenraad R. van den Brom,*[a,b] Ilke Anac,[a] Robert F. Roskamp,[a] Markus Retsch,[a] Ulrich Jonas,*[a,c] Bernhard Menges,[a,d] Jon A. Preece[b]

SUPPORTING INFORMATION

Contents

S1. Characterisation of terpolymer 1 by ^{1}H-NMR spectroscopy

Determination of the composition of the PNIPAAm-based terpolymer **1** is not straightforward. Here, we explain the problem and present the procedure used to successfully prove that terpolymer **1** has the same composition as the initial monomer mixture.

Figure S1 shows a typical ^{1}H-NMR spectrum in methanol-*d*4 of the PNIPAAm-based terpolymer **1**. Independent integration of the CH-peak of the isopropyl group (around 3.9 ppm) and the aromatic CH-peaks of the MABP (around 7.8 ppm) yields the NIPAAm/MABP ratio. Based on this ratio, the amount of methacrylic acid can be calculated from the CH3-peak (around 1.1 ppm). Performing this for a spectrum like in fig. S1 yields a composition of 86 mol% NIPAAm, 5 mol% methacrylic acid and 9 mol% MABP, as was reported previously.[1] However, this is inconsistent with a yield of > 80% and a monomer composition of 94% NIPAAm, 5% MAA and 1% MABP. Interestingly, a copolymer of only NIPAAm and methacrylic acid also yields a spectrum with a peak at the same shift position as the aromatic MABP peak. Therefore, it was suggested that the polymer composition is closer to the composition of the monomer mixture.[2] The increase in the peak intensity around the aromatic peak position (7.4-8 ppm) might be due to a hydrogen bonding interaction between the amide proton of the NIPAAm and the methacrylic acid carbonyl oxygen, which leads to a shift of the amide proton band to the aromatic region.

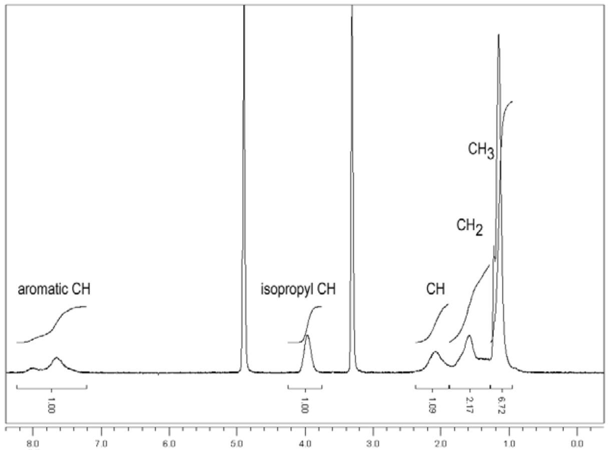

Figure S1. ^{1}H-NMR spectrum of terpolymer **1** in methanol-*d*3

Such amide peaks can be concealed by the addition of deuterium oxide as the amide protons are then exchanged by deuterium. Indeed, in a 1H-NMR spectrum in a mixture of d-methanol, d-chloroform and D_2O the intensity of the broad aromatic peak was significantly decreased and a finer structure typical for MABP became visible (fig. S2, middle).

Further evidence for the hypothesis that the vanished peak can be assigned to an amide was obtained from a high temperature (373 K) 1H-NMR-spectrum of **1** in d-tetrachloroethane (fig S3). Amide and carboxyl peaks are known to shift with temperature, and indeed, only the MABP-related fine-structure is observed around 7.6 ppm under these conditions. Based on the consistency of this result and the spectrum with additional D_2O, it can be stated, that the calculated amount of MABP in the terpolymer in relation to NIPAAm is ~ 1 : 100, in accordance with the monomer feed ratio and contrary to the ratio of ~ 1 : 10 reported earlier.[1]

To check, if the calculated amount of methacrylic acid is correct, the carboxyl group was converted to the corresponding trimethylsilyl (TMS) ester in a polymer analogous reaction. Based on the 1H-NMR-spectrum of this silylated polymer in figure S2 (bottom), the fraction of MAA in the terpolymer was 5 mol% and MABP 1 mol%, respectively. A 1H-NMR-spectrum of the terpolymer with the TMS ester in deuterium oxide was not recorded as D_2O contains tetramethylsilane as reference compound (see Fig. S2 middle), which would prohibit quantitative peak integration. Also note that, since the amide peak did not shift upon the preparation of the TMS ester, it can be concluded that indeed the amide acts as proton donor in the hydrogen bonding interaction with the carbonyl O=C group of the acrylic acid (or TMS ester), which is the acceptor as assumed above.

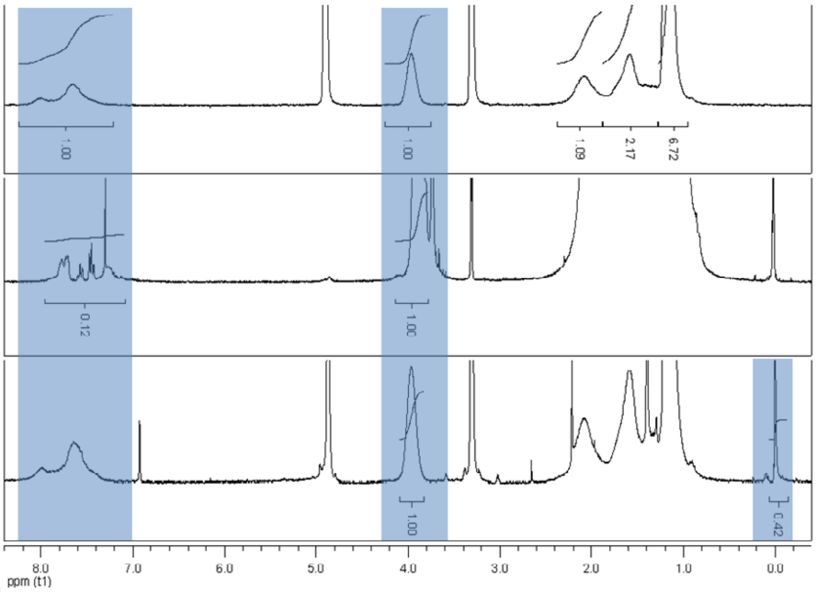

Figure S2 ^{1}H-NMR spectra of terpolymer **1** in methanol-*d*3 (top), in methanol-*d*3 with added chloroform-*d* and deuterium oxide (middle), and of silylated terpolymer **1a** in methanol-*d*3 (bottom)

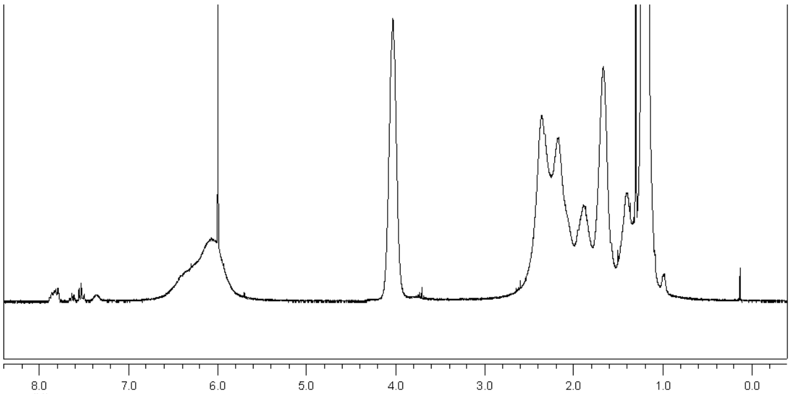

Figure S3 ^{1}H-NMR spectrum of terpolymer **1** in tetrachloroethane-*d*2 at 373K

S1.1. Preparation of the silylated terpolymer 1a

Hexamethyldisilazane (1ml, 4.7 mmol) was added to 85 mg terpolymer **1** at room temperature. After two days all volatiles where distilled of and the silylated polymer **1a** was freeze-dried from *tert*.-butanol.

S1.2. Mechanism of photocrosslinking

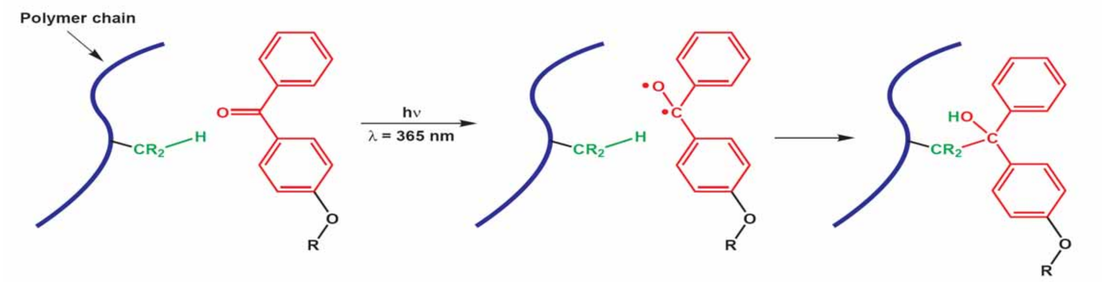

Scheme S1 Benzophenone-based photocrosslinking: UV-irradiation leads to transient formation of a biradical which is capable of insertion into non-aromatic C-H bonds.[3]

S2. Characterisation of functionalised silica nanoparticles 4

S2.1. Scanning electron microscopy

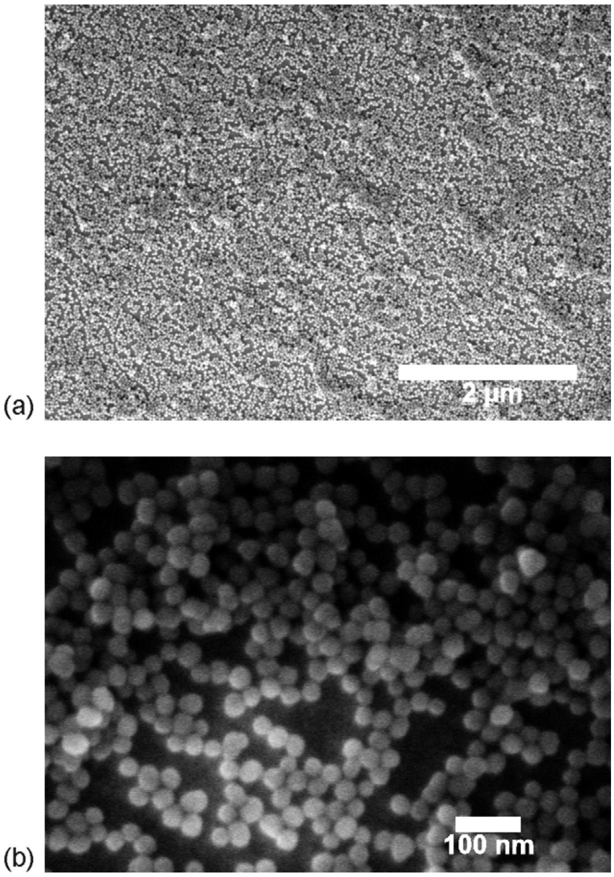

Figure S4 SEM micrographs of BPTES-functionalised, HMDS-passivated silica-nanoparticles **1** that have a diameter of 35 ± 3 nm, as determined by digital image analysis on 80 NPs in (b). (EHT=3.00 kV, WD=2 mm)

S2.2. Determination of the degree of functionalisation of the BPTES-coated NPs

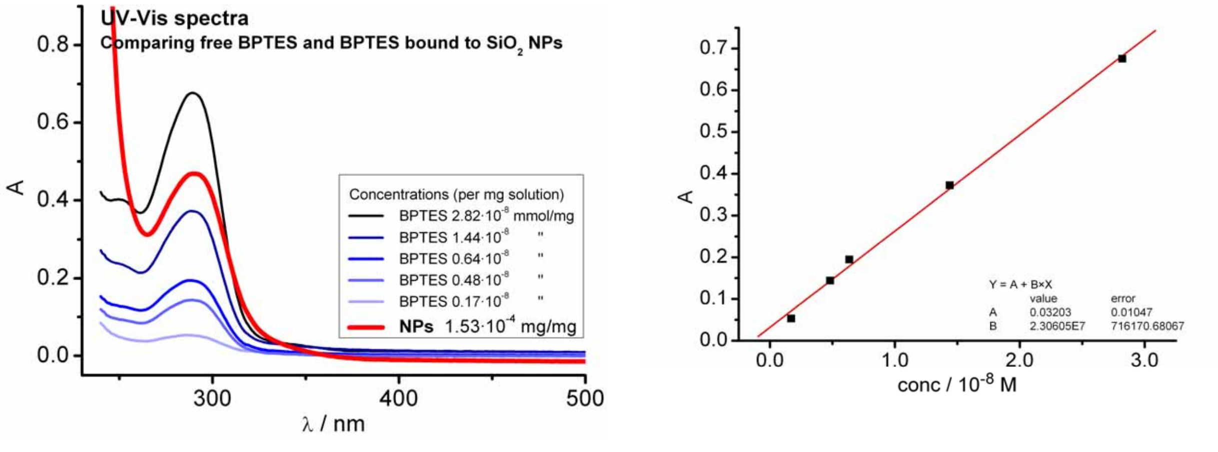

Figure S5 a) UV-Vis absorption spectra of BPTES (**2**) solutions in $CHCl_3$ and (in red) of BPTES-coated nanoparticles (**4**). (b) Calibration curve based on the maximum absorptions (at 288 nm) of the BPTES samples.

S2.2.1. Method/experimental

All spectra were recorded on a Lambda 900 (Perkin Elmer) with a 4 nm slit, 1nm step size and 0.2s integration time. The spectrum of an empty cuvette was used as background for all measurements. The spectrum of neat $CHCl_3$ was subtracted from the BPTES and NP solutions prior to analysis of the BP concentration.

Circa 300μl of an EtOH stock solution of BPTES was concentrated by rotary evaporation and dried in vacuo for >2 h, yielding 20.30 mg of BPTES. This was used to prepare a 3.42 mmol/ml stock solution. Absorption spectra were obtained for a series of 5 different concentrations.

One sample of **4** was taken directly from the $CHCl_3$ stock solution and one sample was diluted with $CHCl_3$ to yield an absorption within the absorption range of the calibration curve. The exact concentration was determined a posteriori by drying an aliquot by rotary evaporation and in vacuo.

A series of calibration spectra of **2** is shown in figure S5a. In fig. S5b, the intensity at the maximum absorption (at 288 nm) is plotted against concentration. A linear fit yields that the absorption A is $A = 0.03 + 2.3\times10^7$ C, where C is in mol/gram.

In figure S5a the absorption of **4** and **2** are compared. It is concluded that the spectra for the free molecules and the nanoparticles are essentially similar, so the intensity (rather than the integral) is a sufficiently accurate measure of the BPTES concentration.

The number of functional groups per particle was calculated based on the average particle diameter obtained from SEM and an estimated density of 1.3 (based on centrifugation results). The resulting number of $(1.2\pm0.1)\times10^{-4}$ $mol\cdot g^{-1}$ (*i.e.* moles BPTES per gram of NPs) corresponds to *ca* $2.0 - 2.3\times10^3$ BP groups per particle (with 35 nm ∅) or to one BP-silane per $1.7 - 1.9$ nm^2 on the surface.

S3. Preparation of composite thin films

S3.1. Details of $CHCl_3$ blends of 1 and 4

TableS 1 Fabrication details for composite films of PNIPAAm and BPTES-functionalised silica NPs

Sample	**Composite composition**	**Blends**		**Photocrosslinking**	
	%-wt NPs	*%-wt in $CHCl_3$*		*dose*	*time*
		HG 1	NP 4	$J \cdot cm^{-2}$	min
A	0	5.73	0.00	6.28	60
B	20	5.75	1.46	6.28	60
C	34	5.77	2.93	6.28	60
D	51	5.43	5.66	6.28	60
E	34	5.77	2.93	3.14	30
F	34	5.77	2.93	1.57	15

S3.2. Larger SEM images of composite films

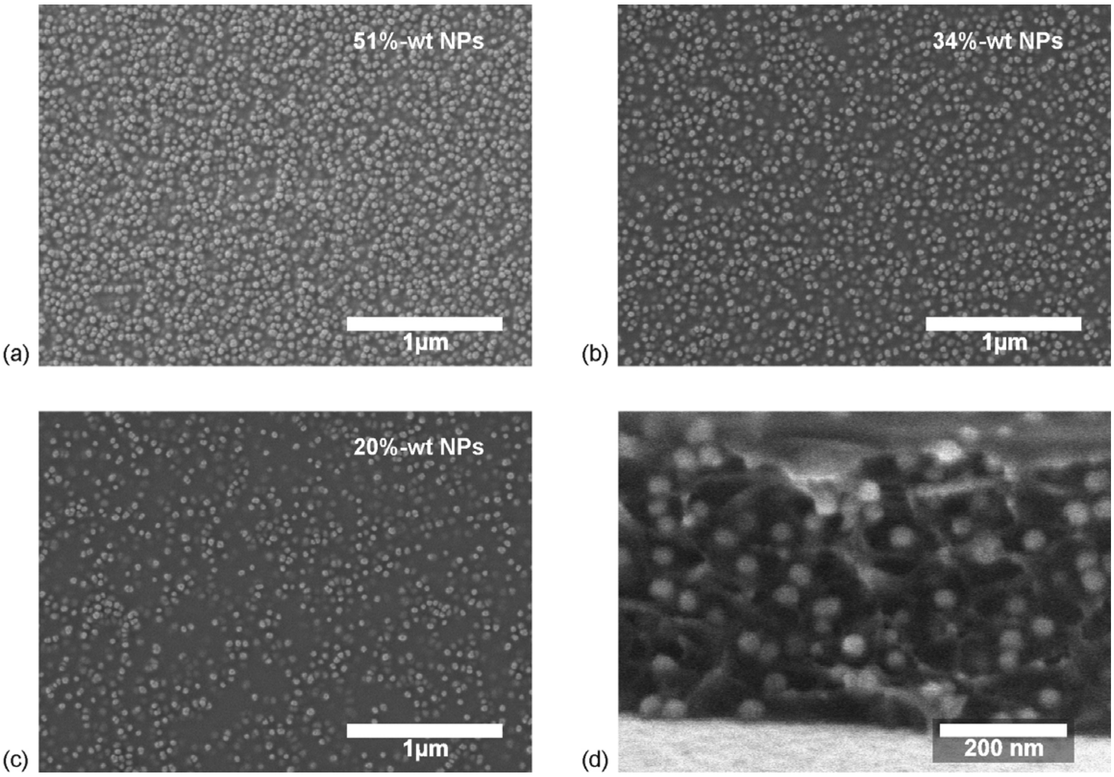

Fig.S6 SEM micrographs of composites of polymer **1** and NPs **4**. (a),(b), and (c) are top views with the NP-content as indicated; (d) shows a cross-sectional image of a film with an NP content of 17%-wt.

S3.3. AFM images of composite films

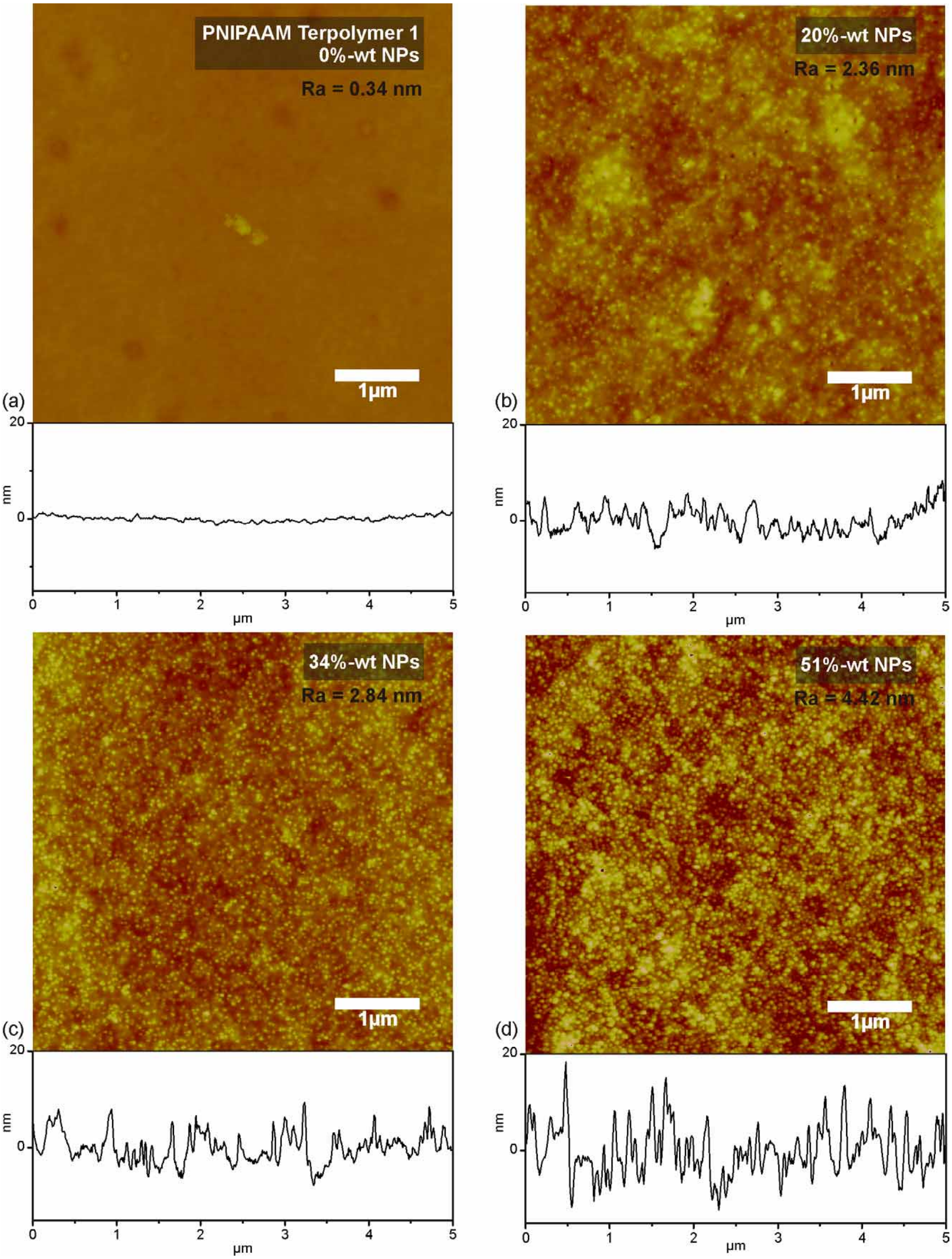

Figure S7 AFM micrographs and cross sections of the PNIPAAm **1** / NP **4** composite films (Samples A–D). Images are 5×5 µm and reproduced with the same colour-height scale.

S3.3.1. Experimental

All AFM micrographs in Fig. S7 were recorded on a Dimension 3100CL scanning probe microscope (Veeco) operated in tapping mode, using Omclac TS160-W2 Al-coated Si cantilevers. The shown cross sections were taken close to the centre of the respective micrographs.

S4. Surface plasmon resonance and optical waveguide spectroscopy

S4.1 Box model simulation of SPR/OWS spectra: Multilayer description

For the samples presented in this paper, the model multilayer system consisted of LaSFN9 glass, chromium (d_{Cr} , ε_{Cr}), gold (d_{Au}, ε_{Au}), thiolate adhesion layer (d_{thiol}, ε_{thiol}), the hydrogel/nanoparticle composite (d_{comp} , ε_{comp}), and solvent (water, ε_{H2O}=1.770).
The parameters of the composite layer were determined by minimising the difference between the modelled and experimental I(θ), varying only d_{comp} , ε'_{comp} and ε''_{comp}. In this procedure the parameters for the substrate and thiol layer were kept constant. These were determined independently during two reference scans, one before the deposition of the thiol layer, and one afterwards (i.e. before spincoating of the composite film). In a typical procedure, ε'_{comp} was first adjusted to match the angles θ of the simulated and experimental first waveguide mode (TM1). Subsequently d_{comp} was adjusted to get a similar match for the last waveguide mode (TMn) and, if necessary, repeating these two steps.

S4.2 Angular scans $I(\theta)$ of samples B and C

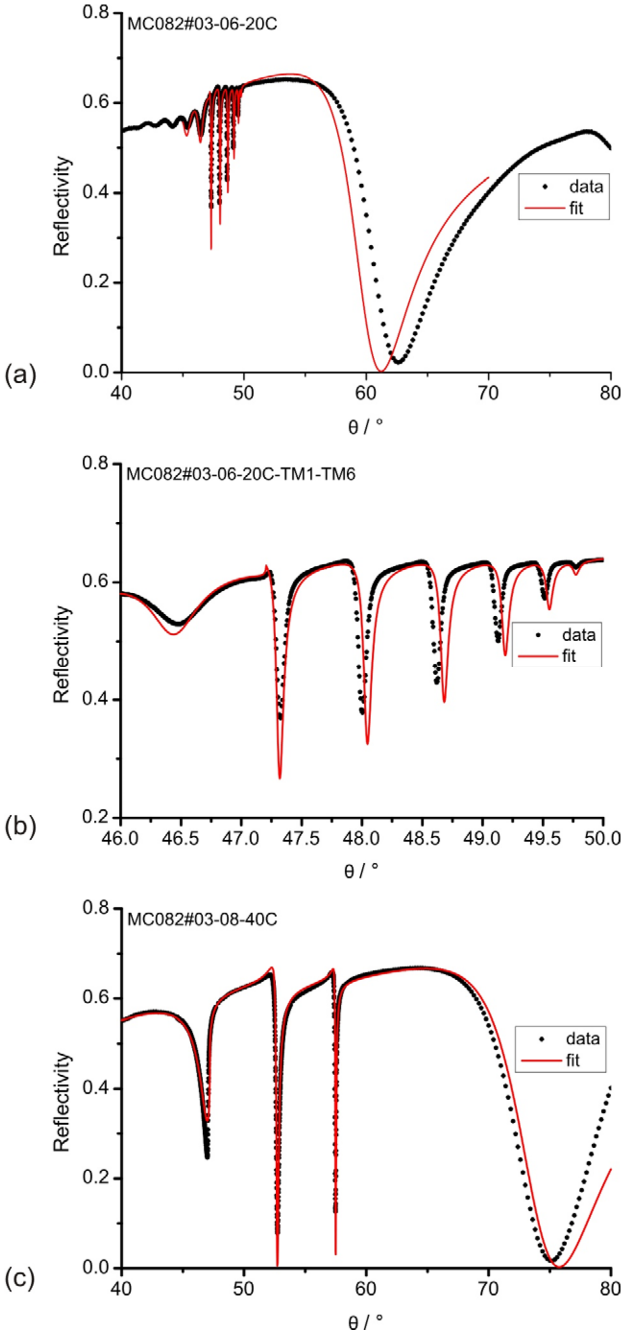

Figure S8 SPR/OWS spectra for sample B: a composite film of PNIPAAm terpolymer **1** and NPs **4** (20%-wt) on an LaSFN9 glass slide with a gold film coated with adhesion promoter **3**, (photocrosslink dose 6.28 J·cm^{-2}).
(a) The film swollen in water at 20 °C. (b) A close up of (a) in the region of the minima corresponding to the guided optical waves TM1 to TM6. (c) The collapsed film in water at 40 °C. All spectra were recorded with *p*-polarised light. The dots are measured data points, the lines correspond to simulated spectra (using a box model - *i.e.* a uniform layer thickness and a single refractive index).

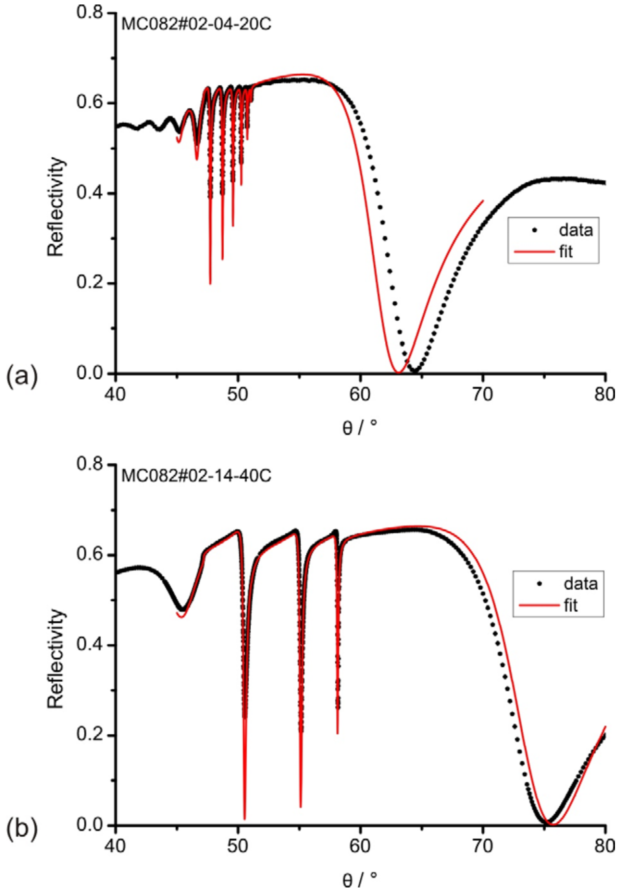

Figure S9 SPR/OWS spectra for sample C: a composite film of PNIPAAm terpolymer **1** and NPs **4** (34%-wt) on an LaSFN9 glass slide with a gold film coated with adhesion promoter **3**, (photocrosslink dose 6.28 J·cm^{-2}).
(a) The film swollen in water at 20 °C. (b) The collapsed film in water at 40 °C. Both spectra were recorded with *p*-polarised light. The dots are measured data points, the lines correspond to simulated spectra (box model - *cf.* Fig S8).

S4.3 The inverse Wentzel-Kramers-Brillouin approximation

The Wentzel-Kramers-Brillouin (WKB) approximation is a well-established method to find field distribution functions for the guided modes in wave guides (slab-shaped) with a refractive index gradient in the *z*-direction.[4] Though details of this method are outside the scope of this paper, a qualitative description will be given here. Solving the wave equation for a guided mode in a slab-shaped waveguide using the WKB-approximation leads to three solutions that are oscillating and evanescent in the *z*-direction, respectively, and which apply in different regions of the film. The former applies in the centre of the film, the latter towards the edge. The two solutions are connected at so-called *turning points*. The turning points for the different modes in a waveguide are at different *z*, because they have different field distributions.

Here, we use a *reversed* WKB approximation, in the sense that we wish to extract RI as a function of *z* from the guided waves obtained from spectra like in fig. 4d in the paper. Thus, for every mode TM1-TM*n* in a given configuration, an effective refractive index n_{eff} (for that mode) and a turning point are obtained. Subsequently, it is assumed that the *physical* RI at the turning point is equal to n_{eff} that is experienced by that particular mode. Although this assumption does not follow directly from the WKB approximation, it is justified by (a) the physical plausibility of these RIs and (b) the good fit of simulated spectra that are based on these profiles to the experimental data (See figure 4c in the paper)

S4.4. Determination of T_cs upon heating and cooling

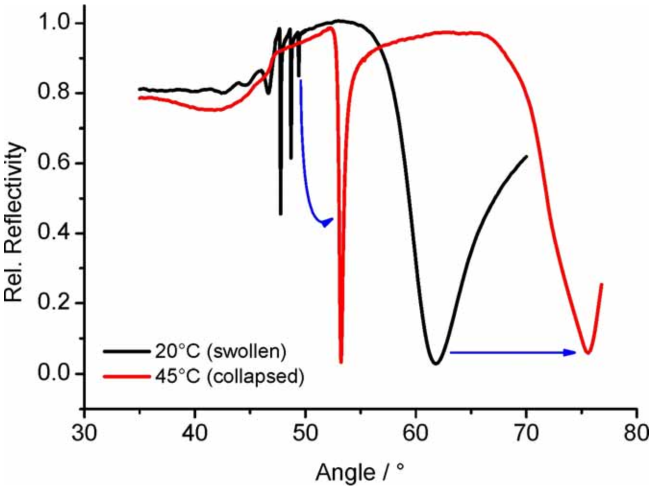

Figure S10 Overlay of SPR/OWS spectra for a PNIPAAm **1** / NP **4** composite film in swollen (20 °C) and collapsed state (45 °C). The arrows depict the shift of TM0 and TM1, respectively. To determine the critical temperature, these shifts are traced whilst ramping the temperature up and down.

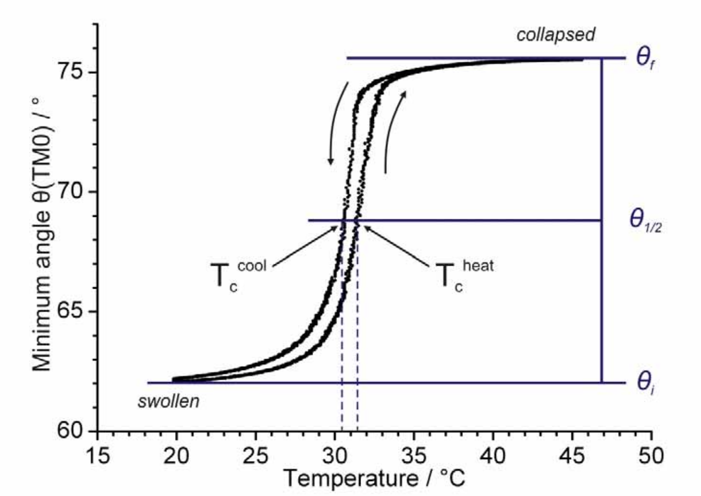

Figure S11 Determination of the critical temperatures from the shift in coupling angle θ(TM*n*) during a temperature cycle. $\theta(T_c) = \{ \theta_f(45\ °C) - \theta_i(20\ °C)\}/2$.

S4.5 Priming of SPR/OWS samples

All samples A–F were primed after installation in the setup, by ramping the temperature from 20 °C up to 45 °C (well above the collapse temperature) and back at least three times. Thus, any unbound polymer or NP fragments are forced out of the film. Comparison of scans of $I(\theta)$ at both 20 °C and 40 °C, recorded during each priming cycle (every time after the temperature had stabilised for 20 minutes) showed that this leads to very stable films with reproducible spectra (see fig S12).

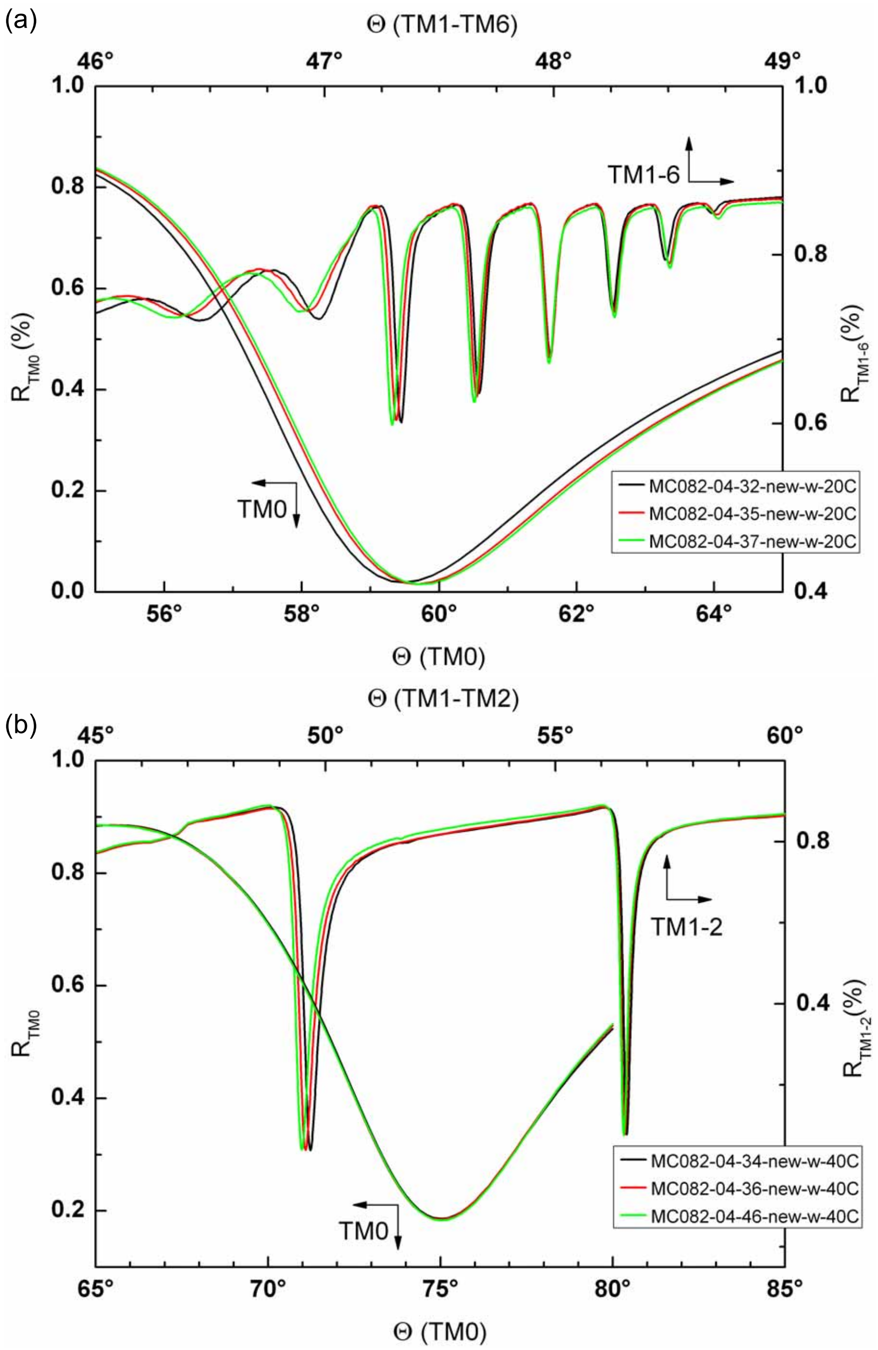

Figure S12 Effect of priming on a hydrogel film. Close-ups of angular scans in the waveguide region (TM1–6) and the surface plasmon region (TM0), (a) for the swollen gel at 20 °C and (b) for the collapsed gel at 40 °C. Scans are shown before priming (black) and after the first and second priming cycles (red and green, respectively).

S4.6 Reproducible swell-collapse cycles

The stability of the composite films is demonstrated by the reproducibility of the response to temperature of a composite film upon repeat cycling of the temperature. The curves in fig S13a and S13b show how the tracks of θ(TM1) during three cycles superimpose fully, both when plotted against temperature and against time.

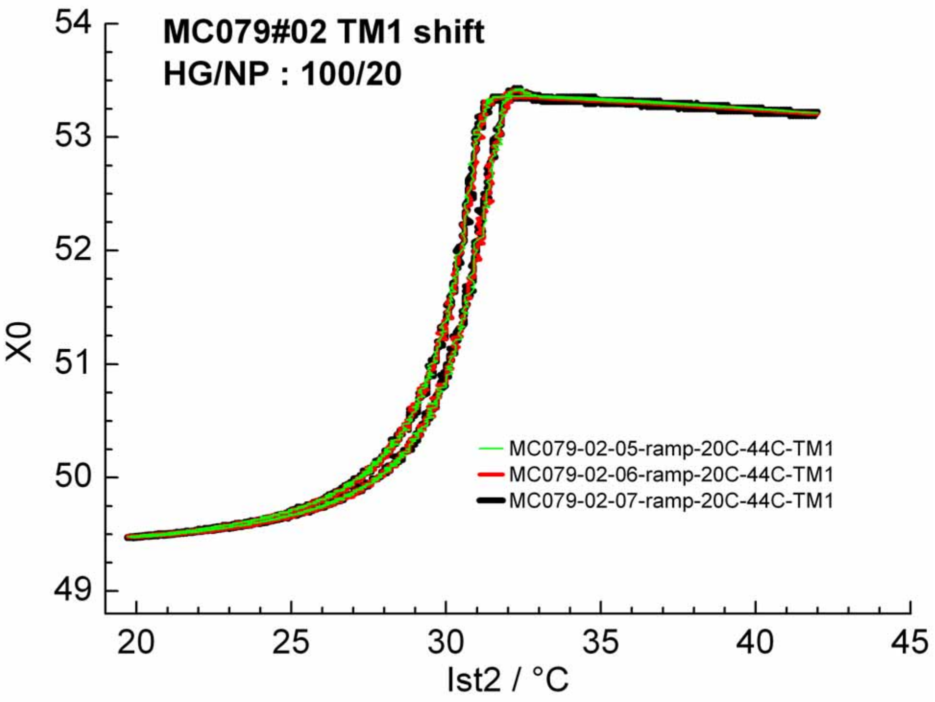

(a)

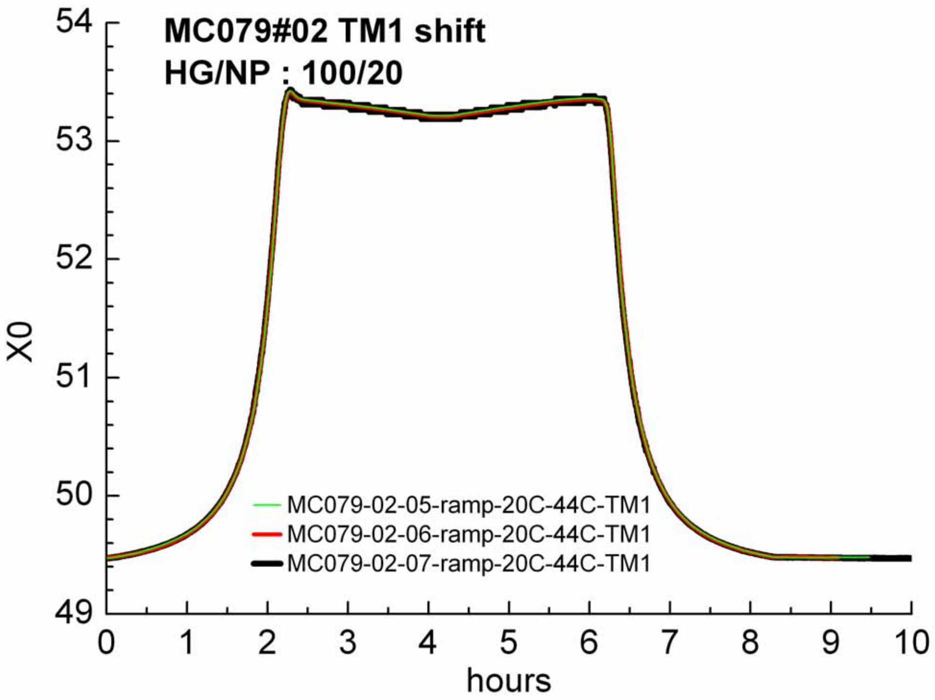

(b)

Figure S13 Minimum tracking curves of θ(TM1) during temperature cycling, (20 °C–44 °C, 0.1K·min^{-1}) for a 700 nm composite film of PNIPAAm **1** and NPs **4** (20%-wt). (a) The angle θ(TM1) as a function of temperature and (b) as a function of time.

S5 Force–distance spectroscopy

S5.1 Scheme showing δ_{ref}, δ_{max}, and δ_0

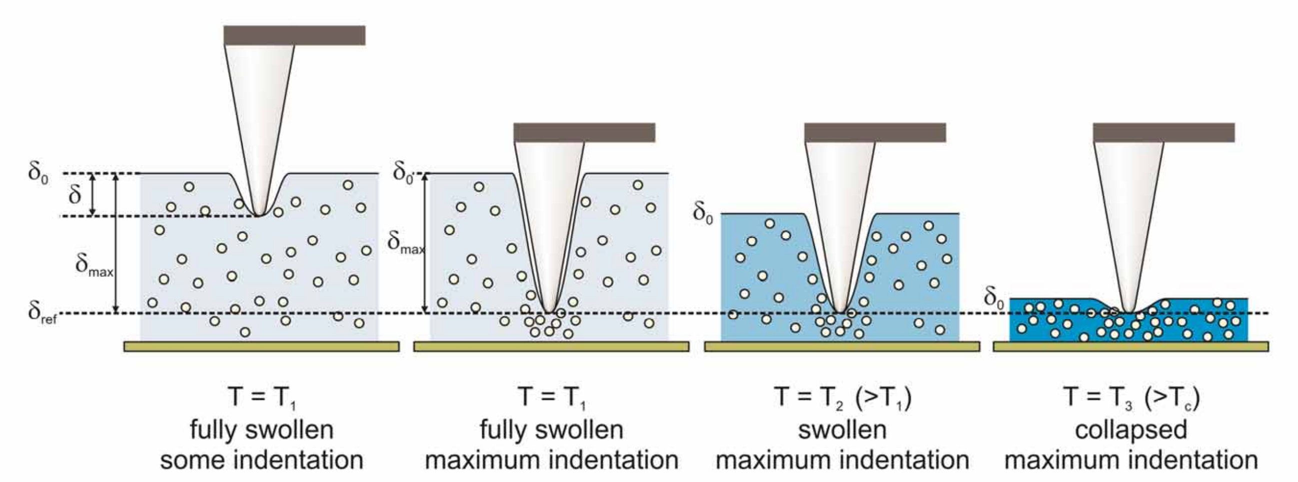

Figure S14 The F–I curves in figure 9 in the paper are aligned based on the assumption that the film is always compressed down to δ_{ref} regardless of temperature. The swelling ratios based on force–indentation curves (SR_{FI}) are hence derived by comparing δ_{max} at different temperatures.

S5.2 Approach and retract curves

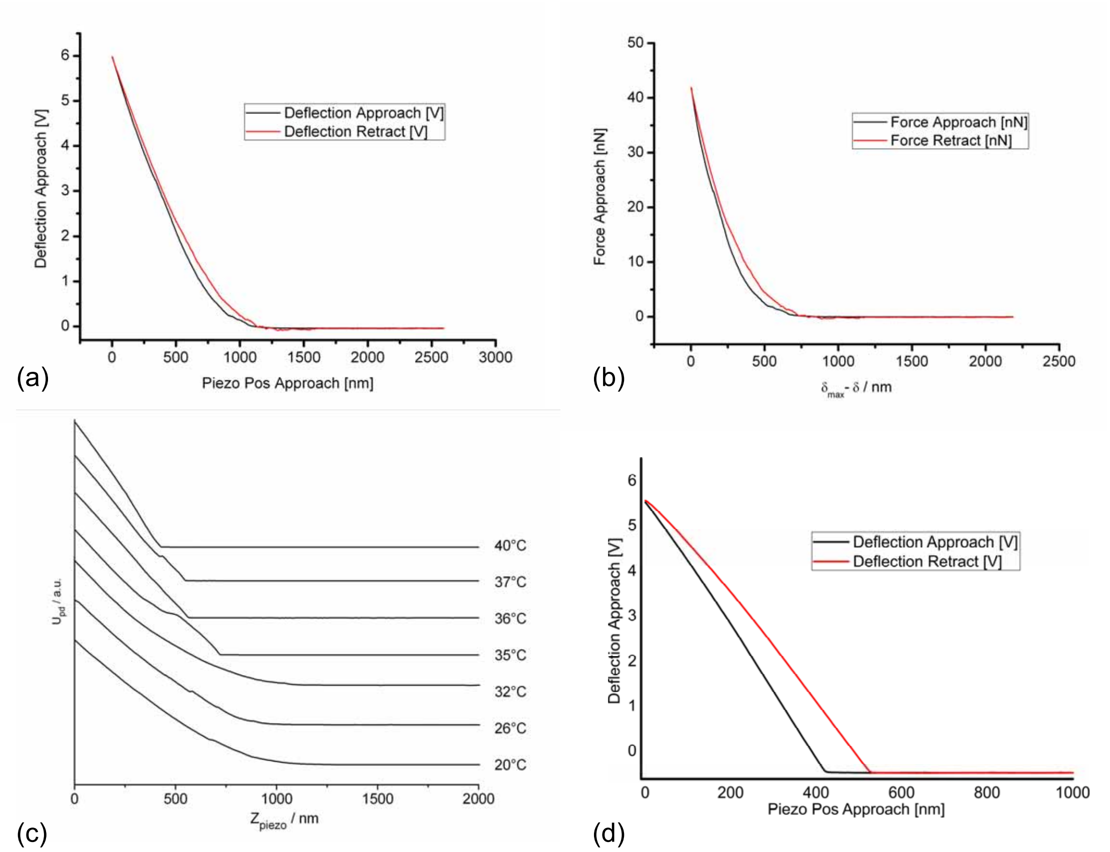

Figure S15 Example of approach and retract curves (a) cantilever deflection vs. scanner position (referenced to maximum scanner position) and (b) corresponding FI-curve for a PNIPAAm **1** / NPs **4** composite film containing 38%-wt NPs, swollen in water at 20 °C; (c) selected cantilever deflection vs. scanner position curves for the same sample at different temperatures (corresponding to the FI curves in Fig. 9); (d) Selected approach and retract cantilever deflection vs scanner position curve recorded at the hard reference surface (the glass substrate). The compliance regime (in this case the entire sloped part of the approach curve), shows a slight deviation from linearity, probably caused by non-linearity of the photodiode and additional buckling of the cantilever at large deflections.

S5.3 Example of Hertz-model fits

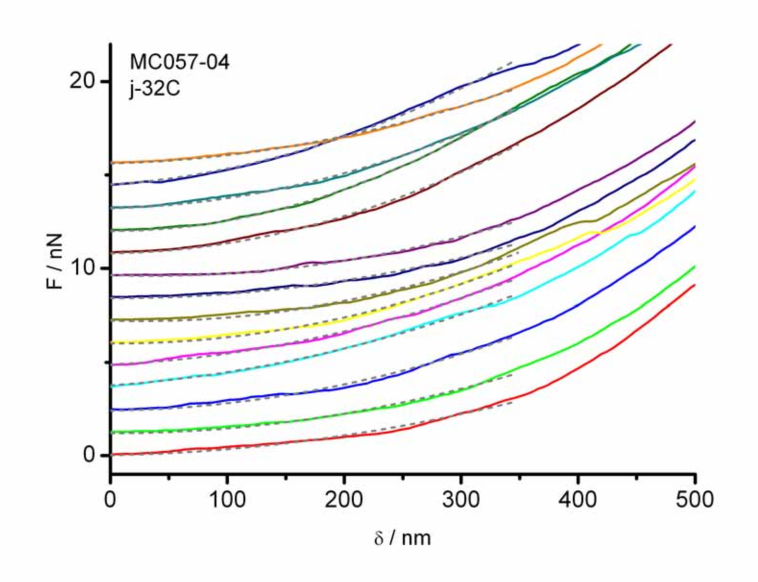

Figure S16 Example of Hertz-model fits (described in the paper) to FI-curves at 32 °C for a PNIPAAm **1** / NPs **4** composite film containing 38%-wt NPs. The grey dotted lines represent the fits. These fits yield an average E-modulus of 60 ± 16 kPa.

S6. References

1. P. W. Beines, I. Klosterkamp, B. Menges, U. Jonas and W. Knoll, *Langmuir*, 2007, **23**, 2231-2238.
2. M. J. N. Junk, U. Jonas and D. Hinderberger, *Small*, 2008, **4**, 1485-1493.
3. N. J. Turro, *Modern Molecular Photochemistry*, University Science Books, 1991, Mill Valley, CA, 1991.
4. W. Karthe and R. Müller, *Integrierte Optik*, Akad. Verlagsges. Geest & Portig, Leipzig, 1991.